Cylindrical Terrain Classification using a Compliant Robot Foot with a Flexible Tactile-Array Sensor for Legged Robots

Pongsiri Borijindakul[1,2,3], Noparit Jinuntuya[1], Alin Drimus[2], and Poramate Manoonpong[2,3]

[1] Kasetsart University, Bangkok, Thailand
[2] Embodied AI & Neurorobotics Lab, Centre for Biorobotics, The Mærsk Mc-Kinney Møller Institute, University of Southern Denmark, Odense, Denmark
[3] Institute of Bio-inspired Structure and Surface Engineering, Nanjing University of Aeronautics and Astronautics, Nanjing, China
prince_jai-yen@hotmail.com, fscinpr@ku.ac.th, drimus@mci.sdu.dk, poma@mmmi.sdu.dk

Abstract. In this paper, we present a new approach that uses a combination of a compliant robot foot with a flexible tactile-array sensor to classify different types of cylindrical terrains. The foot and sensor were installed on a robot leg. Due to their compliance and flexibility, they can passively adapt their shape to the terrains and simultaneously provide pressure feedback during walking. We applied two different methods, which are average and maximum value methods, to classify the terrains based on the feedback information. To test the approach, We performed two experimental conditions which are 1) different diameters and different materials and 2) different materials with the same cylindrical diameter. In total, we use here eleven cylindrical terrains with different diameters and materials (i.e., a 8.2-cm diameter PVC cylinder, a 7.5-cm diameter PVC cylinder, a 5.5-cm diameter PVC cylinder, a 4.4-cm diameter PVC cylinder, a 7.5-cm diameter hard paper cylinder, a 7.4-cm diameter hard paper cylinder, a 5.5-cm diameter hard paper cylinder, a 20-cm diameter sponge cylinder, a 15-cm diameter sponge cylinder, a 7.5-cm diameter sponge cylinder, and a 5.5-cm diameter sponge cylinder). The experimental results show that we can successfully classify all terrains for the maximum value method. This approach can be applied to allow a legged robot to not only walk on cylindrical terrains but also recognize the terrain feature. It thereby extends the operational range the robot towards cylinder/pipeline inspection.

Keywords: Compliant robot foot · Flexible tactile-array sensor · Cylindrical terrains.

1 Introduction

Currently, walking robots are widely employed for locomotion on complex terrains as well as terrain classification [1,2]. While classifying flat and rough terrains are typical ones for the robots [3-9], classifying cylindrical terrains are still under investigation. Tactile sensing is one of the core sensing methods and the most useful technique for object exploration and terrain recognition [10,11]. It has been widely used in robot hands to classify different shapes, materials, and surfaces [12-14]. Therefore, in this work, we apply a flexible tactile-array sensor to a robot leg with a bio-inspired compliant foot to classify different types of cylindrical terrains during walking. There is a variety of cylinder terrains, for instance, water pipes, gas pipes, wires, and so on. If a robot can classify or recognize the terrains during moving or walking on them, it would be useful for adaptation to the terrains as well as terrain/object inspection. In the following section, we present the robot leg with the compliant foot. Section 3 provides neural locomotion control of the leg for walking on different cylindrical terrains. Section 4 introduces the flexible tactile array sensor that provides pressure feedback. Section 5 describes the experimental setup and methods for terrain classification. Sections 6 and 7 gives the experimental results and the conclusion of this work, respectively.

2 Robot Leg with a Bio-Inspired Compliant Foot for Walking on Cylindrical Terrains

We have developed a robot leg based on a hind leg of the dung beetle which has an interesting structure for both locomotion and curved object transportation. The leg has three active joints and three segments (coxa, femur, and tibia) between the joints. The segments are simplified and designed by following the proportion of the hind leg (i.e., coxa: femur: tibia is 1: 1.2: 1, see Fig. 1(a) and [1] for more details). The lengths of the coxa, femur, and tibia parts are 7 cm, 8.4 cm, and 7 cm, respectively. They are printed using 3D-printing. The CT- and FT-joint rotate around the z-axis while the TC-joint rotates around the x-axis. These rotations follow the joint rotations of the real dung beetle leg. The base of the TC-joint is attached to a linear slide allowing the leg freely move in a vertical direction during a stance phase. A flexible cable is used to hold the leg during a swing phase for ground clearance. We have simplified the robot foot by using a fin-ray inspired concept which compliancy mimics the segmented structure of the real tarsus of the beetle. It consists of five rays/blades embedded inside its triangular structure (Fig. 1(a)). It is printed using 3D-printing with a compliant material (i.e., rubber). Although this design does not fully capture the complete complex structure of the tarsus of the dung beetle, it, as an abstract version, shows flexibility and compliance to passively adapt its shape to follow the contour of a substrate as observed in the beetle. Besides the passive adaptation, the compliant foot also acts as a damping system to reduce contact force when the leg touches the ground, see more in [1].

3 Neural Locomotion Control

The concept of central pattern generators (CPGs) for locomotion has been studied and used in several robotic systems of particular walking robots. There is a wide variety of different CPG models available ranging from detailed biophysical models to pure mathematical oscillator models. Here, the model of a CPG for basic locomotion of robot leg is realized by using the discrete-time dynamics of a simple 2-neuron oscillator network (Fig. 1(b)). Due to its neurodynamics, it is able to autonomously generate various periodic and chaotic signals without sensory feedback; i.e., it can act as open-loop control. For our implementation here, the activity of each neuron develops according to $a_i(t+1) = \sum_{j=1}^{n} W_{ij} o_j(t);\ i = 1, ..., n$ with an update frequency of 20 Hz, where n denotes the number of units. The neuron output o_i is given by a hyperbolic tangent (tanh) transfer function $o_i = \tanh(a_i) = \frac{2}{1+e^{-2a_i}}$ -1 . W_i is the synaptic strength of the connection from neuron j to neuron i. The two neurons $H_{0,1}$ of the CPG are fully connected with the four synapses W_{00}, W_{01}, W_{10}, W_{11} and can form an oscillator if the weights are chosen according to an SO(2)-matrix:

$$\mathbf{W} = \begin{pmatrix} W_{00} & W_{01} \\ W_{10} & W_{11} \end{pmatrix} = \alpha \begin{pmatrix} cos(\varphi) & sin(\varphi) \\ -sin(\varphi) & cos(\varphi) \end{pmatrix}, \tag{1}$$

with $-\pi < \varphi < \pi$ and $\alpha > 1$, the oscillator generates sine-shaped periodic outputs $o_{0,1}$ of the neurons $H_{0,1}$ (Fig. 1(c)) where φ defines a frequency of the output signals. In order to achieve stable locomotion (or stepping pattern), we here set φ to 0.5 and α to 1.01 and use a CPG postprocessing unit to shape the CPG signals. The resulting signals $M_{TC,CT,FT}$ drive the motors of the leg (Fig. 1(d)). With this setup, the neural controller acts as an open-loop controller to control the leg. We use this control setup to generate a walking pattern of the leg on cylindrical terrains investigated here [1].

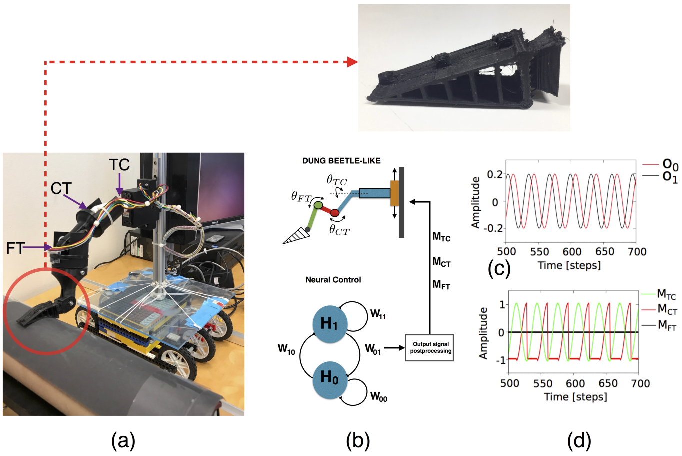

Fig. 1: (a) A robot leg with bio-inspired (fin ray) compliant foot. (b) CPG-based neural control for locomotion. It consists of two interconnected neurons $H_{0,1}$. (c) Outputs $o_{0,1}$ of the neurons $H_{0,1}$ of the CPG-based control. (d) Motor signals $M_{TC,CT,FT}$ obtained from a CPG output signal postprocessing unit. The post processing unit translates the outputs $o_{0,1}$ into the proper motor signals.

4 Flexible Tactile Array Sensor

The piezoresistive material has been chosen as the most suited to build a flexible tactile-array sensor. The tactile sensor is built as an array of 10 x 25 taxels (tactile cells) within 16 mm x 40 mm responsive to pressure applied normally. A range of other sensor configurations were built previously and detailed information can be found in [2,15]. Each tactile cell exhibits decreased resistance for increased pressure with the resistance varying from 1 MΩ in the uncompressed state to under 1 kΩ in the stressed state. The pressure tactile sensor is composed of 3 layers overlaid, where the middle layer is a piezoresistive rubber, while the upper and lower layers being rows and columns of flex printed PCB wired perpendicularly. A multiplexing scheme based on the voltage divider principle implemented with dedicated electronics addresses all combinations of rows and columns and transforms them into a tactile image of 250 elements, each value being an 8-bit value. A second layer is added to the pressure sensor for sensing curvature based on the Spectra Symbol technology for measuring flexing of the material. Bending this sensor increases the resistance which is added to the tactile image of pressure information. The dedicated electronics module stream the information over wifi providing 30 frames per second of distributed pressure together with curvature information as shown in Fig. 2(a).

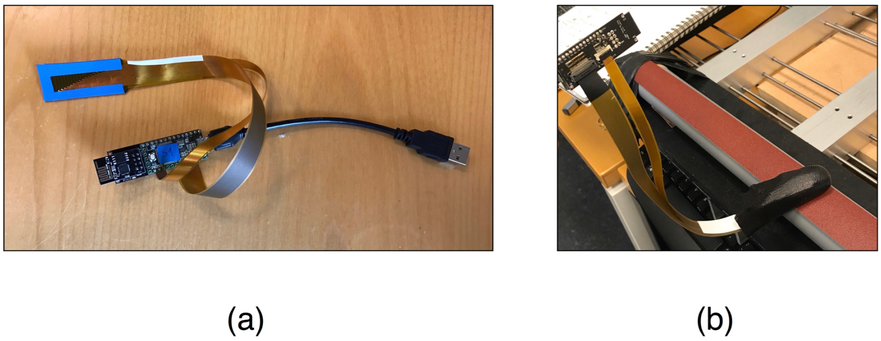

Fig. 2: (a) A flexible wireless tactile array sensor. (b) A compliant foot with a tactile array sensor covered by a rubber glove.

5 Experimental Setup and Methods for Terrain Classification

We implemented a compliant robot foot and a tactile array sensor together by fixing a tactile array sensor under a compliant foot. The robot foot was covered by a rubber glove for having a friction while the robot is walking as shown in Fig 2(b). The leg was attached to a moving cart which was constrained by two rails, to ensure that the leg moves along the terrains during locomotion[1]. We divided the experiment into two conditions. For the first condition, we provided the different diameters and different terrains. The setup of the leg with a cart to investigate locomotion efficiency on cylinder terrains with 3 different terrains and 5 different diameters which are a 8.2-cm diameter PVC cylinder (PVC A), a 4.4-cm diameter PVC cylinder (PVC B), a 7.4-cm diameter hard paper cylinder (Hard Paper), a 20-cm diameter sponge cylinder (Sponge A), and a 15-cm diameter sponge cylinder (Sponge B), was setup as shown in Fig 3. The second condition, we provided the identical diameter with 3 different terrains which are a 7.5-cm diameter PVC cylinder (PVC A), a 5.5-cm diameter PVC cylinder (PVC B), a 7.5-cm diameter sponge cylinder (Sponge A), a 5.5-cm diameter sponge cylinder (Sponge B), a 7.5-cm diameter hard paper cylinder (Hard Paper A), and a 5.5-cm diameter hard paper (Hard Paper B) as shown in Fig 4. In this experiment, the tests take 10 steps, 5 times on each terrain. For each terrain, 50 tests were done, averages on each terrain resulting in 50 trials in total. Figure 5 shows contact area on each step while the compliant robot foot walks on each terrain. We can determine the contact area during walking through pressure intensity on the heat maps. The green colour shows low pressure, the blue colour shows medium pressure, and the white colour shows high pressure on each area. The red colour means no foot contact.

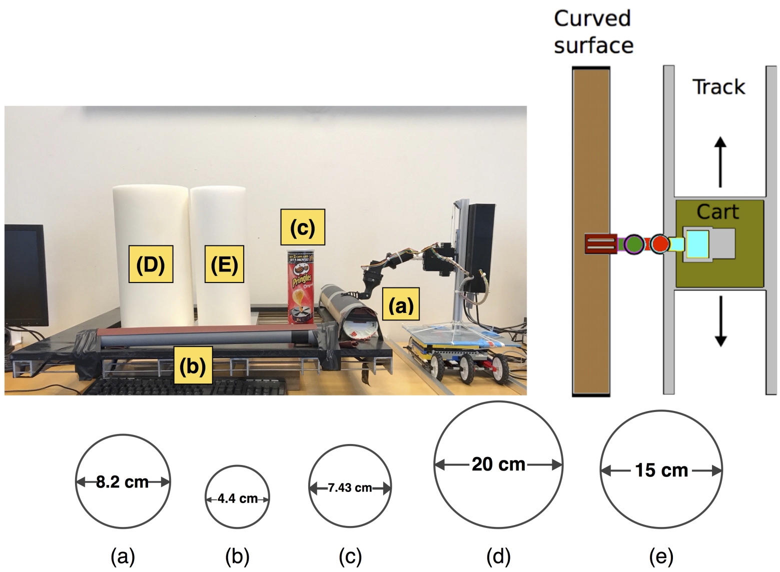

Fig. 3: Experimental set-up of the leg system for locomotion of the first experiment on cylindrical terrains which are (a) PVC A, (b) PVC B, (c) Hard Paper, (d) Sponge A, and (e) Sponge B.

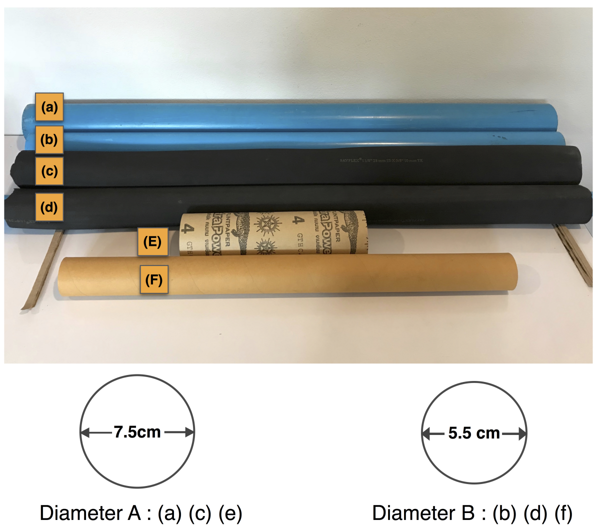

Fig. 4: Six different kinds of cylindrical terrains of the second experiment which are (a) PVC A, (b) PVC B, (c) Sponge A, (d) Sponge B, (e) Hard Paper A, (f) Hard Paper B.

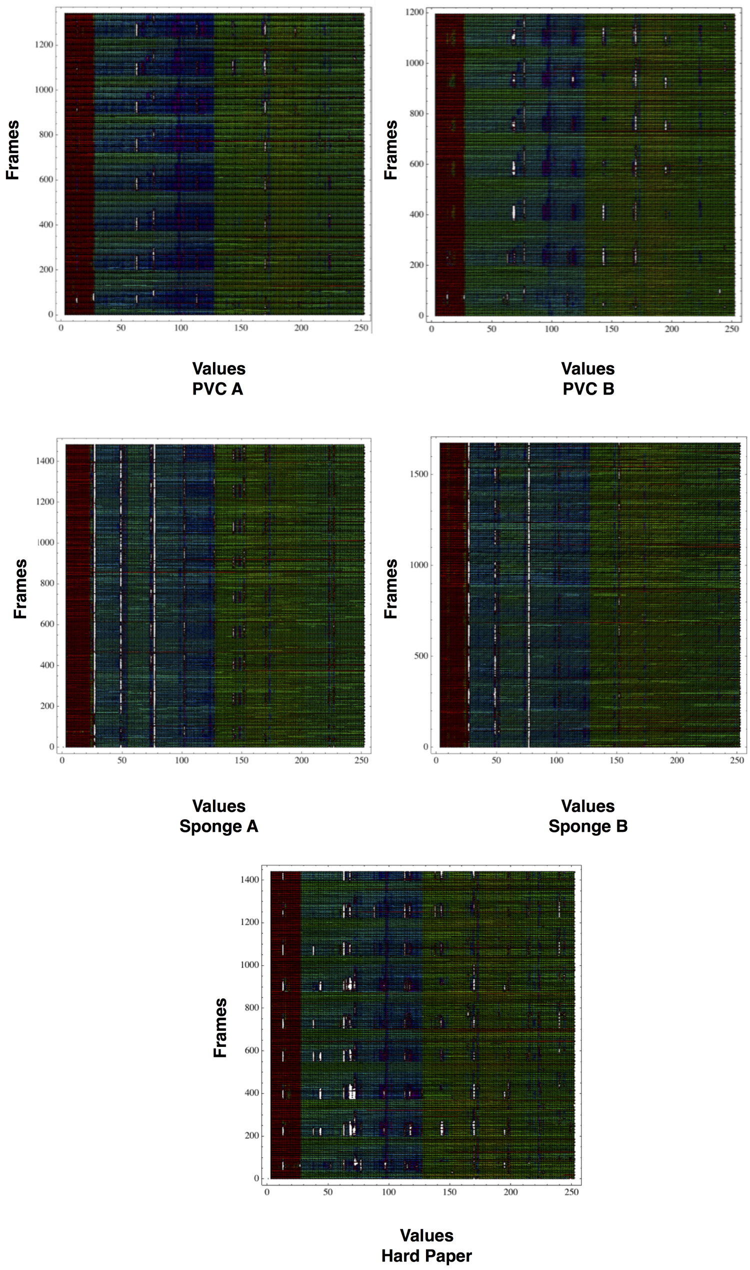

Fig. 5: Examples of heat maps of the tactile array sensor on each step while the compliant robot foot walks on each terrain. we encourage the reader to see the videos of the experiments at http://www.manoonpong.com/SAB2018/.

5.1 Average Value Method

According to the experiment, the tests take 10 steps, 5 times on each terrain. We calculated the averages of each step, which means we got 50 values of the averages on each terrain. We also calculated the standard deviation for calculating the expanded uncertainty using metrology method. The 50 average values have been divided into half (25:25). The second half was tested using the data of the first half. We demonstrated the correction of classification by doing the confusion matrix (Tables 1,3).

5.2 Maximum Value Method

In this method, we calculated the maximum values on each step, which means we also got 50 values on each terrain. we have calculated the standard deviation for calculating the expanded uncertainty using metrology method as well. The 50 maximum values have been divided into half (25:25). The second half was tested using the data of the first half. We demonstrated the correction of classification by doing the confusion matrix (Tables 2,4).

6 Experimental Results

On the first experiment, the average method classification shows some mistakes as shown in Table. 1. There are two terrains have a percentage of correction under 50, noticeably the Hard Paper has a percentage of correction equal to 0. Moreover, there are three terrains have 32 percentage of unknown values which are unidentified because of the overlap of the values. Therefore, the average value method cannot be used for cylindrical terrain classification. By contrast, the maximum value method shows that (Table. 2) all of the materials are able to classify by using this method, especially, on large diameter materials (PVC A and Sponge A). They have a percentage of correction over 90. On the second experiment, we divided the terrains into two groups, which are Diameter A (7.5-cm) group and Diameter B (5.5-cm) group. The average method classification shows the huge mistakes almost every terrains accept Sponge B and every terrains have the unidentified value as shown in Table. 3. Therefore, the average value method cannot be used for cylindrical terrain classification. By contrast, the maximum value method shows that (Table. 4) all of the terrains are able to classify by using this method. The clear diagonal for maximum value method confirms the successful recognition. Therefore, this method is suited for the cylindrical terrain classification. According to the classification, we found that for the same terrains different diameters, a gap of the averages of maximum value between these materials will be small. On the other hand, if terrains are different whether diameters are same or different, a gap of the averages of maximum value between these terrains will be outstanding. We also can identify the difference of terrains by hard terrains have an average maximum value less than soft terrains as shown in Figs. 6 and 7. For hard terrains, the bigger diameter has an average less than the smaller, but for soft terrains, the bigger diameter has an average more than the smaller. Moreover, we found that the more hardness of terrains, the less uncertainty. The reason is while a compliant robot foot is walking on hard terrains, there is no deformation of terrains but for soft terrains, there is a deformation on each step and the hardness on each point are different. The uncertainty of the average of maximum values was calculated by using metrology method for precise calculation.

Table 1: Confusion matrix of the first experiment of average value method for cylindrical terrain classification. The vertical axis represents the truth and the horizontal represents the output of the classification in percentage.

AV Method						
Object	PVC A	PVC B	Hard Paper	Sponge A	Sponge B	Unknown
PVC A	88	12	0	0	0	0
PVC B	8	72	0	0	20	0
Hard Paper	8	0	0	4	56	32
Sponge A	0	0	0	96	0	4
Sponge B	0	8	4	36	20	32

Table 2: Confusion matrix of the first experiment of maximum value method for cylindrical terrain classification. The vertical axis represents the truth and the horizontal represents the output of the classification in percentage.

MV Method						
Object	PVC A	PVC B	Hard Paper	Sponge A	Sponge B	Unknown
PVC A	91.67	8.33	0	0	0	0
PVC B	0	64	36	0	0	0
Hard Paper	0	20	80	0	0	0
Sponge A	0	0	0	92	4	4
Sponge B	0	0	0	28	68	4

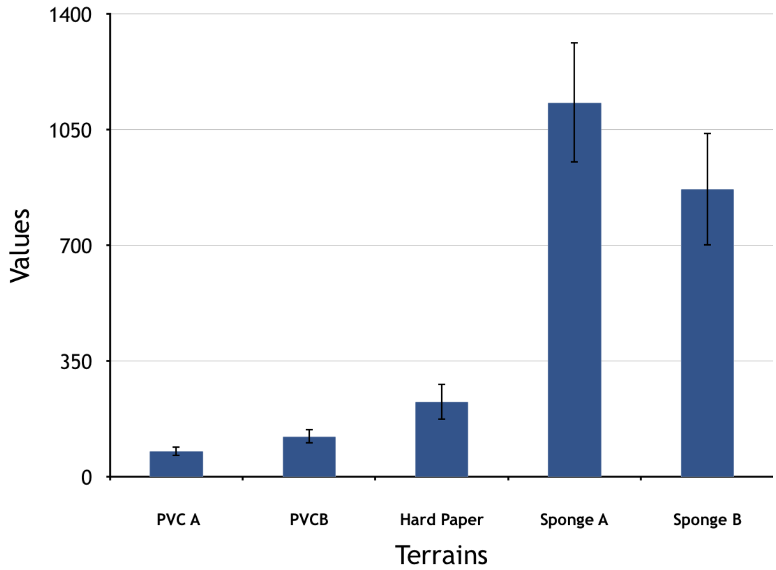

Fig. 6: Comparison chart of the first experiment of the average of maximum values while the compliant robot foot walks on each terrain.

Table 3: Confusion matrix of the the second experiment of average value method for cylindrical terrain classification. The vertical axis represents the truth and the horizontal represents the output of the classification in percentage.

AV Method				
Diameter A				
Object	PVC A	Hard Paper A	Sponge A	Unknown
PVC A	0	80	0	20
Hard Paper A	0	40	20	40
Sponge A	0	68	4	28

AV Method				
Diameter B				
Object	PVC B	Hard Paper B	Sponge B	Unknown
PVC B	12	0	60	28
Hard Paper B	40	0	56	4
Sponge B	20	0	72	8

Table 4: Confusion matrix of the second experiment of maximum value method for cylindrical terrain classification. The vertical axis represents the truth and the horizontal represents the output of the classification in percentage.

MV Method				
Diameter A				
Object	PVC A	Hard Paper A	Sponge A	Unknown
PVC A	81	19	0	0
Hard Paper A	10	65	25	0
Sponge A	0	25	75	0

MV Method				
Diameter B				
Object	PVC B	Hard Paper B	Sponge B	Unknown
PVC B	62	28	10	0
Hard Paper B	24	76	0	0
Sponge B	4	25	71	0

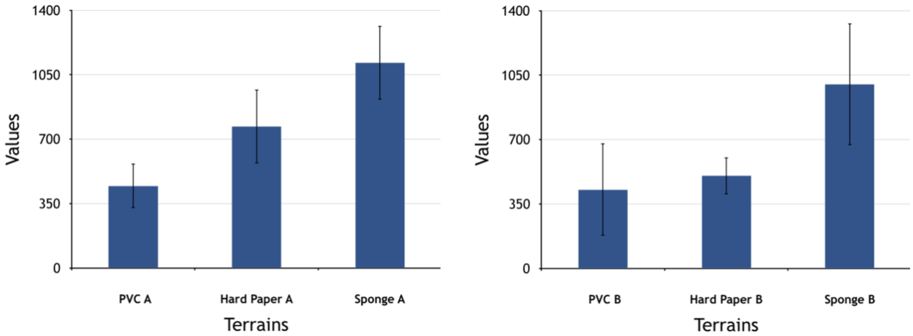

Fig. 7: Comparison chart of the second experiment of the average of maximum values while the compliant robot foot walks on each terrain.

7 Conclusion

In this study, we presented the combined usage of a compliant robot foot with a flexible tactile sensor array for cylindrical terrain classification. We performed two conditions in the experiment which are 1) different diameters and different terrains and 2) different terrains with the same diameter. Two different methods were used which are average and maximum value methods. We found that the suitable method for cylindrical terrain classification is maximum value method. We also can identify a different kind of materials or diameters by comparing the averages of the maximum value. In order to improve classification performance, two legs could be used as complementary to tactile sensing. Walking robots will be able to recognize terrains while they are walking, explore, and adjust their suitable walking pattern on different terrains in future.

8 Acknowledgements

This work was supported by The Capacity Building on Academic Competency of KU. Students from Kasetsart University, Thailand, Centre for BioRobotics (CBR) at University of Southern Denmark (SDU, Denmark), and the Thousand Talents program of China.

References

1. Di Canio, G., Stoyanov, S., Larsen, J.C., Hallam, J., Kovalev, A., Kleinteich, T., Gorb., S.N., Manoonpong, P.: A robot leg with compliant tarsus and its neural control for efficient and adaptive locomotion on complex terrains. Artificial Life and Robotics **21**(3), 274–281 (2016)
2. Drimus, A., Kootstra, G., Bilberg, A., Kragic, D.: Design of a flexible tactile sensor for classification of rigid and deformable objects. Robotics and Autonomous Systems **62**, 3–15 (2014)

3. Mrva, J., Faigl, J.: Feature Extraction for Terrain Classification with Crawling Robots. Robotics 2010 Current and Future. J. Yaghob (Ed.), ITAT 2015, pp. 179–185, Charles University in Prague, Prague, (2015)
4. Walas, K.: Terrain Classification and Negotiation with a Walking Robot. Intelligent & Robotic Systems **78**(3-4), 401–423 (2015). https://doi.org/10.1007/s10846-014-0067-0
5. Degrave, J., Van Cauwenbergh, R., wyffels, F., Waegeman, T., Schrauwen, B.: Terrain Classification for a Quadruped Robot. Machine Learning and Applications (ICMLA), IEEE, Miami(2013). https://doi.org/10.1109/ICMLA.2013.39
6. L. Garcia Bermudez, F., C. Julian, C., W. Haldane, W., Abbeel, P., S. Fearing, R.: Performance Analysis and Terrain Classification for A Legged Robot Over Rough Terrain. Intelligent Robots and Systems, IEEE/RSJ, Vilamoura(2012). https://doi.org/10.1109/IROS.2012.6386243
7. Belter, D., Skrzypczy?ski, P.: Rough Terrain Mapping and Classification for FootholdSelection in a Walking Robot. Field Robotics **28**(4), 497–528 (2011). https://doi.org/10.1002/rob.20397
8. Kisung, K., Kwangjin K., Wansoo, K., Seungnam, Y., Changsoo H.: Performance Comparison between Neural Network and SVM for Terrain Classification of Legged Robot. SICE Annual Conference 2010, pp. 1343–1348. IEEE, Taipei(2010).
9. Poppinga, J., Birk, A., Pathak., K.: Hough Based Terrain Classification for Realtime Detection of Drivable Ground. Field Robotics **25**(1), 67–88 (2008). https://doi.org/10.1002/rob.20227
10. Alice Wu, X., Myung Huh, T., Mukherjee, R., Cutkosky, M.: Integrated Ground Reaction Force Sensing and Terrain Classification for Small Legged Robots. IEEE Robotics and Automation Letters **1**(2), 1125–1132 (2016)
11. Walas, K.: Tactile Sensing for Ground Classification. Journal of Automation, Mobile Robotics & Intelligent Systems **7**(2), 18–23 (2013)
12. Gong, D., He, R., Yu, J., Zuo., G.: A Pneumatic Tactile Sensor for Co-Operative Robots. Sensors **17**(11), 2592–2606 (2017)
13. Jamali, N., Sammut, C.: Material Classification by Tactile Sensing using Surface Textures. Robotics and Automation, pp. 2336–2341. IEEE, Anchorage(2010). https://doi.org/10.1109/ROBOT.2010.5509675
14. Nakamoto, H., Kobayashi, F., Kojima, F.: Shape Classification using Tactile Information in Rotation Manipulation by Universal Robot Hand. Robotics 2010 Current and Future Challenges, Houssem Abdellatif (Ed.), ISBN : 978-953-7619-78-7.
15. Drimus A., Mtfi-Tempfli S. Tactile Shoe Inlays for High Speed Pressure Monitoring. In: Liu H., Kubota N., Zhu X., Dillmann R., Zhou D. (eds) Intelligent Robotics and Applications. ICIRA 2015. Lecture Notes in Computer Science, vol 9245. Springer, pp. 74–81. Springer, Cham(2015). https://doi.org/10.1007/978-3-319-22876-1_7